A Simple Tool for Modeling Microstrip Structures using the Finite-Difference Time-Domain Method

Xisto L. Travassos Jr, Walter P. Carpes Jr[1], Adriano C. Lisboa and Elson J. Silva[2].

Abstract—**This work presents a simple tool for modeling microstrip structures based on the finite difference time domain (FDTD) technique. This is the start of an effort to construct oriented object software for the simulation of microwave structures using the FDTD method. Three simulations of microstrip structures are presented and three kinds of absorbing boundary conditions (ABC's) are implemented.**

Index Terms—**FDTD, grid-mesh generation, microstrip structures.**

I. INTRODUCTION

The Finite-Difference Time-Domain (FDTD) method is undoubtedly the most popular numerical method for the solution of problems in electromagnetics. Although the FDTD method has existed for over 30 years, its popularity continues to grow as computing costs continue to decline [1].

The application of the FDTD to model microstrip problems is not new. Reineix and Jecko [2] were the first to apply the FDTD method to the analysis of microstrip antennas assuming an appropriate choice of excitation to find the frequency dependence of the relevant parameters using Fourier transform of the transient current.

However, there are some limitations in applying the FDTD to practical problems. One major difficulty when using this technique is the description of the geometrical components of the device under test in the computational domain. This task of describing the geometrical details is a very time consuming process, especially if programmed by the designer for every individual case. The optimal solution is to implement a tool that creates and displays device details and transfers geometrical information to the FDTD engine.

The problem to be addressed requires the development of a FDTD application instead of a FDTD program. The difference between an application and a program is that a program can be used to simulate one specific problem; but an application can be used for an infinite number of user-defined problems.

In this work, a tool has been created where the designer can model the shape of an arbitrary microwave structure defining the points of the mesh that are composed by dielectric or conductors materials.

II. PROBLEM DESCRIPTION AND MESH GENERATION

The first step in the application development is to define how to describe the microstrip problem, *i.e.* geometry and physical properties. Region interfaces - with cardinality k (number of edges) - are represented by a Planar Straight Line Graph (PSLG) [3], where nodes store their own position, and edges store start/end node indices and left/right region labels (see Fig. 1).
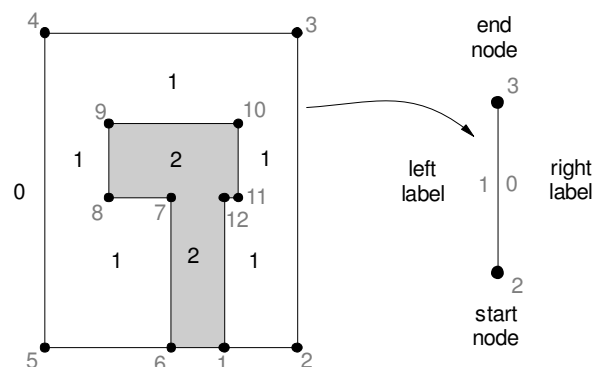

Fig. 1. Geometry description.

Only x-grid - with cardinality n_x - and y-grid - with cardinality n_y - are stored, not all nodes positions of the mesh (see Fig. 2). This scheme reduces a great deal the need for storage space - $O(n_x+n_y)$ instead of $O(n_x n_y)$ -, while keeping a constant time $O(1)$ to access the coordinates of nodes of an element.

The trick to access nodes without having the mesh itself consists in adopting a numbering scheme for the elements. By convention, it was chosen left to right, bottom to up precedence starting from zero. The first element of the grids is also indexed with zero. For instance, the coordinates of the first node of the i-th element would be the integer division of i by n_x-1 in y-grid, and its remainder in x-grid. Note that this does not depend on the grids content, only on their cardinality, which is much like accessing elements of a matrix.

Nevertheless, matching an element to a region can be done only in time $O(\log k)$ (after some domain pre-processing),

which could slow down mesh access. Thus it is pre-assigned a region label to each element, so that this operation can be done in time O(1). Note that this requires a storage $O(n_x n_y)$.
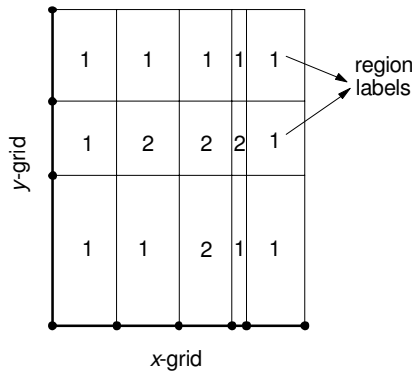

Fig. 2. Mesh description.

To assign region labels, it is applied a sweep algorithm [3], as shown in Fig. 3. Note that the geometry is constrained to be axis aligned, which simplify the algorithm.

Firstly, a line sweeps out all y-axis interval centers. Each time this line starts crossing a segment, this is added to a list L of active segments. It is removed from L when the sweep line ends crossing it. The list L contains the segments right label sorted by the segment x position, which are event points to an x-axis sweep line. This line sweeps x-axis interval centers, assigning labels to elements. The current label is initiated with zero and, each time the x-sweep line crosses an event point, it is updated.

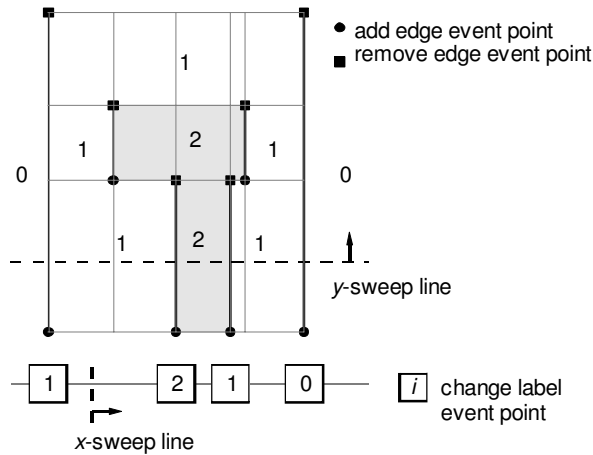This algorithm runs in time $O(k \log k + n_x n_y)$.

Fig. 3. Sweep algorithm to assign regions to elements.

All mesh generation described here are independent on the contents of the x and y-grids. In the current application, each grid is composed by equally sized intervals, Δx and Δy, as shown in Fig. 4.

In microstrip context, generally there are only two kinds of region: dielectric and conductor. Therefore, a single bit (or maybe a few of them) could be used to distinguish regions, in order to save storage space. Nonetheless, a simple integer

(32bits long in most computer platforms) is very suitable to work with, while having virtually no limit to the number of different regions.
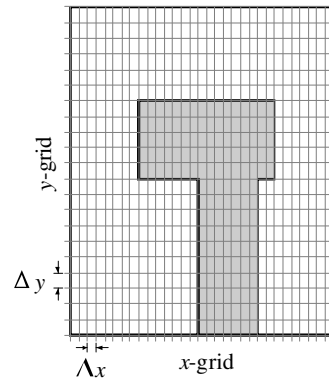

Fig. 4. Grid generation.

III. FDTD METHOD AND ABSORBING BOUNDARY CONDITIONS

A. Finite Difference Time Domain Method

In 1966, Kane Yee originated a set of finite-difference equations for the time-dependent Maxwell's curl equations systems for the lossless materials case. Since then the FDTD technique has been widely used in electromagnetic computations. In this method, Maxwell's equations are discretized both in time and space by using the central difference scheme. The central difference technique reduces the round-off error for accuracy to the second order. With time and space discretized, the electric and magnetic fields are interlaced within the spatial 3-D grid.

Nevertheless, open problems involving theoretically boundless space extension can be only solved by applying special conditions on the boundaries that permit all outward-propagating numerical waves to exit as if the simulation were performed on a computational domain of infinite extent.

In the process, the outer-boundary condition must suppress spurious reflections of the outgoing numerical waves to an acceptable level, permitting the FDTD solution to remain valid for all time-steps, specially after the reflected numerical wave return to the vicinity of the modeled structure [4].

To absorb the outgoing waves, the ABC's can be simulated in a number of ways. These are classified as analytical (or differential) ABC and material ABC. The material ABC is realized from the physical absorption of the incident numerical wave by means of a lossy medium, whereas the analytical ABC is simulated by approximating the wave equation on the boundary. Some absorbing boundary conditions are analyzed next.

B. Description of three Boundary Conditions

1. *Mur's first approximate absorbing condition* [5]

The first technique appears with the one-way approximation of the numerical wave developed by Engquist-Madja. Based in this formulation, Mur created the standard ABC of the 1980's implementing partial derivatives as numerical central differences expanded about an auxiliary grid-point assuming that if a plane wave is normally incident on a planar surface, and if the surface is perfectly absorbing, there will be no reflected wave.

Solving the differential equation for a numerical wave traveling along the negative *x* direction and imposing that this wave is incident on the planar surface and that should not be reflected, an absorbing condition for a normally incident wave is found.

$$\frac{\partial U(x,t)}{\partial x} = \frac{1}{c} \frac{\partial U(x,t)}{\partial t} \Bigg|_{x=\frac{\Delta x}{2}, t=\left(n+\frac{1}{2}\right)\Delta t} \qquad (1)$$

This equation can be written in finite-difference form averaging the values at the half grid points and half time steps that are not available in the algorithm as

$$U_0^{n+1} = U_1^n + \left(\frac{c\Delta t - \Delta x}{c\Delta t + \Delta x}\right)\left(U_1^{n+1} - U_0^n\right) \qquad (2)$$

This equation is known as the second order accurate 1st order Mur's ABC and can be used for updating the fields on the outer boundary of the interior region. However, this technique is not faultless. In fact, a wave is absorbed without reflection only in the particular case of normal incidence. For oblique incidence, however, a portion of the wave energy will be reflected.

One disadvantage of the Mur's ABC is that we must set boundaries sufficiently far from the scatterer when solving interaction problems to reduce the level of imperfections in the simulation.

2. *Higdon boundary operator*

The Mur's ABC annihilates a normally incident wave highly accurately. However, for obliquely incident waves, large reflections can occur. In order to improve the accuracy for ABC's derived from the one-way equation, other boundary operators have been introduced to annihilate waves at multiple angles. The Higdon operator [6] consists in a differential annihilator for a superposition of plane waves traveling toward the $x = 0$ boundary, each one with a relative incident angle. Considering this, Higdon proposed the annihilator function for this sum of plane waves in the form

$$\left[\prod_{l=1}^{L}\left(\cos\phi_l \frac{\partial}{\partial t} - c\frac{\partial}{\partial x}\right)\right]U = 0 \qquad (3)$$

This operator annihilates any combination of plane waves propagating at the angles ϕ_l. In addition, this operator does not require space derivatives parallel to the grid outer boundary. Thus, the stencil of grid-points needed to implement the Higdon operator is one-dimensional in the direction perpendicular to the grid boundary. This simplifies the numerical implementation, especially near the corners of rectangular grids [4].

Considering the second operator (*L*=2) and discretizing time and space derivatives at a half-cell, as done previously with the Mur's ABC, and introducing a damping term [7], leads to

$$U_M^n = -(\kappa_1 + \kappa_2)\left(U_{M-1}^n - U_M^{n-1}\right)$$
$$-\kappa_1\kappa_2\left(U_{M-2}^n + U_M^{n-2}\right) + \left((\beta+1) + 2\kappa_1\kappa_2\right)U_{M-1}^{n-1} \qquad (4)$$
$$+(\beta\kappa_2 + \kappa_1)\left(U_{M-2}^{n-1} - U_{M-1}^{n-2}\right) - \beta U_{M-2}^{n-2}$$

where

$$\kappa_i = \frac{1-\rho_i}{1+\rho_i(1+\alpha_1\Delta x)}, \ \rho_i = \frac{c\Delta t}{\cos\phi_i\Delta x},$$
$$\beta = \frac{1+\rho_i}{1+\rho_i(1+\alpha_1\Delta x)} \qquad (5)$$

The damping term is due to the disadvantage of the Higdon operator that can be unstable in the late time.

3. *Uniaxial Perfectly Matched Layer* [8]

The UPML is a material ABC implemented by surrounding the computational domain with a lossy medium that dampens the outgoing fields. This method overcomes the Berenger PML as it uses the Maxwelliam formulation, with no need to split the field components. As a result, additional memory and processor efforts are minimized. The strategy of this technique is to assume a time-harmonic arbitrarily plane wave propagating in an isotropic medium incident on a material half-space described as a uniaxial anisotropic medium having the permittivity and permeability tensors

$$\overline{\overline{\varepsilon}} = \begin{bmatrix} a & 0 & 0 \\ 0 & a & 0 \\ 0 & 0 & b \end{bmatrix} \overline{\overline{\mu}} = \begin{bmatrix} c & 0 & 0 \\ 0 & c & 0 \\ 0 & 0 & e \end{bmatrix}, \qquad (6)$$

and to determine the constitutive parameters for which $\Gamma = 0$ for all angles of incidence. It was demonstrated in [8] that the plane wave will be purely transmitted into the uniaxial medium when $a = c = b^{-1} = e^{-1}$. Due to the discontinuity at the interface, a large reflection can occur due to the discretization error. This error can be minimized by spatially scaling the conductivity profile in the absorbing medium as

$$\sigma(x) = \left(\frac{x}{d}\right)^m \sigma_{max}, \qquad (7)$$

where d is the depth of the PML, m is the order of the polynomial variation and σ_{max} is chosen to achieve a determined reflection error. It has been found that for a large class of applications, an optimal choice of σ_{max} for polynomially scaled PML with 10 and 5 cells thick is

$$\sigma_{opt} = \frac{(m+1)}{150\pi\sqrt{\varepsilon_r}\,\Delta x}. \qquad (8)$$

It has been found that the UPML medium can result in reflection errors as minute as –80dB when applied to microstrip structures [4].

IV. NUMERICAL RESULTS

Using the mesh generation tool and the ABC's discussed above, we have studied the influence of this techniques on the input characteristics of a rectangular microstrip patch antenna presented in [9].

In the microstrip structures examined here, the propagating waves are close to the TEM case. The time transient port voltage V can therefore be obtained from numerical integration of eletric field at the antenna terminals according to

$$V = \int \vec{E} \cdot d\vec{l}. \qquad (9)$$

As the FDTD algorithm used is based on total field calculations, the resulting quantities are composed of reflected and incident waves and therefore cannot be directly used for the extraction of scattering parameters.

To obtain the incident waveform, the simulation is performed only with the microstrip line, which will be simulated with an infinite extent.

The resulting voltages (total and incident) recorded at every time step can now be used for extraction of the reflection waveform by subtracting the incident waveform from the total field. The return loss S_{11} can then be obtained by simply applying the Fourier transform on these transient waveforms recorded in port 1 as

$$S_{11}(\omega) = \frac{V_{ref}(\omega)}{V_{inc}(\omega)}. \qquad (10)$$

The input impedance Z_{in} of the antenna is calculated using the return loss as

$$Z_{in} = Z_0 \frac{1 + S_{11}e^{j2kL_a}}{1 - S_{11}e^{j2kL_a}}, \qquad (11)$$

where k is the wavenumber on the microstrip, L_a is the length from the edge of the antenna to the reference plane ($10\Delta y$), and Z_0 is the characteristic impedance of the microstrip line, which is assumed to have a constant characteristic impedance of 50 Ω [10]. Bandwidth is an important characteristic of antennas that is usually referred in terms of fractional bandwidth. The equation for fractional bandwidth is defined as

$$B_w = \left(\frac{F_U\big|_{10dB} - F_L\big|_{10dB}}{F_R}\right) \times 100, \qquad (12)$$

where F_U is the upper frequency where the return loss crosses –10dB and F_L is the lower frequency of a –10dB crossing. The term F_R is the resonant frequency of the antenna, at which the return loss is a minimum. The results for the ABC's mentioned are discussed next.

A. Rectangular Microstrip Patch Antenna

The first structure designed by our tool was the microstrip patch antenna whose geometry and dimensions are shown in Fig. 5. The simulations were performed using a time step $\Delta t = 0.441$ps and space steps $\Delta x = 0.389$mm, $\Delta y = 0.400$mm, $\Delta z = 0.265$mm; the mesh dimensions have different configurations according to the ABC used.
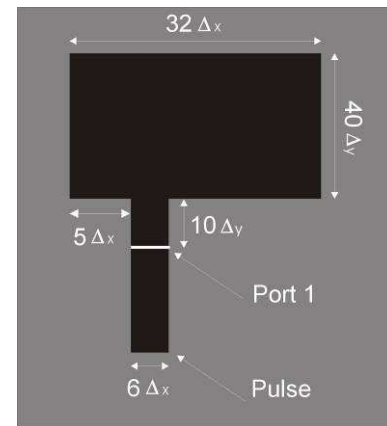

Fig. 5. Microstrip patch antenna dimensions.

The return loss for the considered ABC's is shown in Fig. 6 along with measurement results obtained by Sheen [9].

The results displayed in Fig. 6 show that significant changes in the return loss occurred due to the use of different ABC's in this simulation.
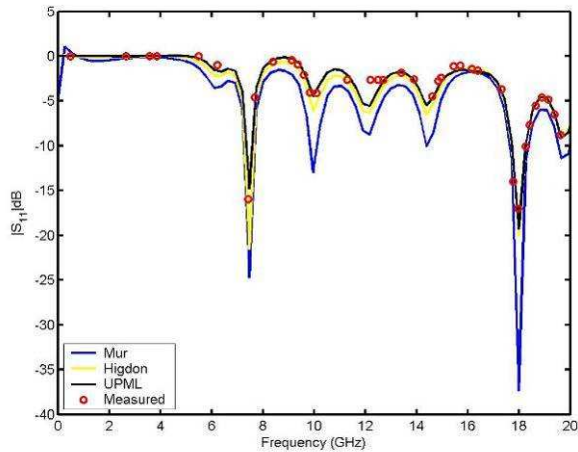
Fig. 6. Return Loss of the Microstrip Patch Antenna with different ABC's.

The results obtained numerically, however, have the penalty of excluding the conductor and dielectric losses in the calculation. Besides, Sheen reported that the network analyzer used to measure the scattering coefficient presented some errors that occurred due to microstrip-to-coaxial transitions, which are not de-embedded in the measurement [9][10]. The results of numerically simulation and the measured values are compared in Table I and Table II.

TABLE I
RETURN LOSS AT THE RESONANT FREQUENCY

ABC	Return Loss (dB)	Relative Error (%)
Mur	−24.7626	55.1497
Higdon $\phi_1=\phi_2=0°$	−21.5270	34.8770
UPML	−18.0986	−7.1712

TABLE II
EVALUATION OF INPUT PARAMETERS AT THE RESONANT FREQUENCY

ABC	Input Impedance (Ω)		Bandwidth (%)
	R	X	
Mur	44.58	−0.71	5.8110
Higdon $\phi_1=\phi_2=0°$	56.21	−6.41	5.0751
UPML	67.27	−12.68	3.2329

B. Microstrip Filter

The second structure modeled was a low-pass filter. The dimensions are shown in Fig. 7. The space steps used are $\Delta x = 0.4064$mm, $\Delta y = 0.4233$mm and $\Delta z = 0.265$mm; the ABC used was the ten cells thick UPML. The time step used is $\Delta t = 0.441$ps and the simulation was performed for 4000 time steps.
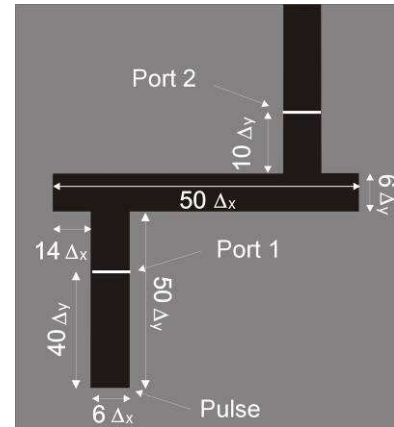

Fig. 7. Low-pass filter dimensions.

The results for the scattering coefficients are shown in Fig. 8 are in good agreement with [8]. The insertion loss is computed using the port 2 that registered only the total field.
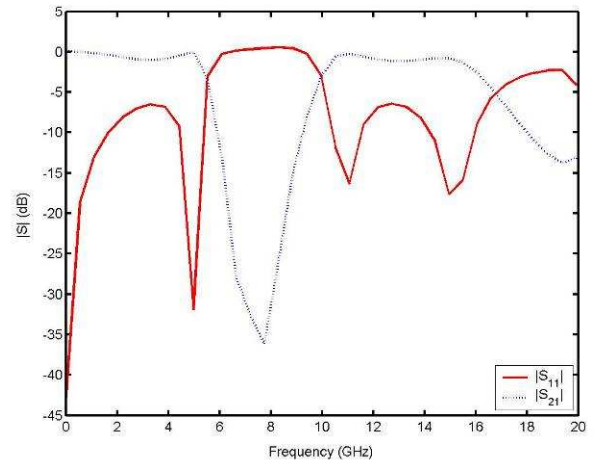

Fig. 8. Return Loss (S_{11}) and Insertion Loss (S_{21}) of the low-pass filter.

C. Microstrip Branch Line Coupler

The third structure modeled was the branch line coupler, shown in Fig. 9, which is used to divide power equally between ports 3 and 4 from ports 1 or 2. This occurs at the frequency where the center-to-center distance between the four lines is a quarter wavelength. To model this circuit, Δx, Δy and Δz are chosen to match the dimensions of the circuit.

The space steps used are $\Delta x = 0.406$mm, $\Delta y = 0.406$mm and $\Delta z = 0.265$mm, with $\Delta t = 0.441$ps. The simulation was performed for 4000 time steps to allow the response on all four ports to become nearly zero.
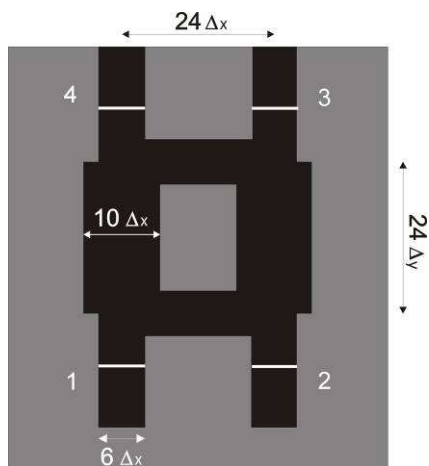
Fig. 9. Branch line coupler dimensions.

The desired branch line coupler performance is seen in the sharp S_{11} and S_{21} nulls that occur at approximately the same point as the crossover in S_{31} and S_{41}. Fig. 10 shows the scattering parameters of the branch line coupler.
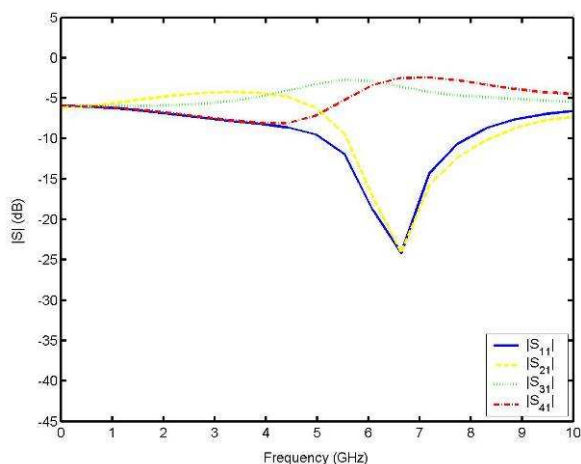

Fig. 10. Scattering parameters of the branch line coupler.

V. CONCLUSIONS

Numerical simulations of some microwave structures designed by our tool and utilizing the finite-difference time-domain method with several absorbing boundary conditions are demonstrated. The computed results are compared with measured data and found to be in good agreement. This paper demonstrates that the FDTD method is very useful for the computer-aided design of many different types of microwave structures.

REFERENCES

[1] Shlager, K. L., and J. B. Schneider, "A Selective Survey of the Finite Difference Time Domain Literature," IEEE Trans., APM-37, No. 4, 1995, pp. 39-56.
[2] Reineix, A. and and B. Jecko, "Analysis of microstrip patch antennas using finite difference time domain method," IEEE Trans. Antennas Propagat., vol. 37, pp. 1361-1369, Nov. 1989.
[3] M. De Berg et.al. "Computational Geometry – Algorithm and Applications", 2nd edition, Springer, 2000.
[4] Taflove, A. e Hagness, S., "Computational Electrodynamics: The finite-difference time-domain method," Artech House, Norwood, MA, 2000.
[5] G. Mur, "Absorbing Boundary Conditions for the Finite-Difference aproximation of the time-domain electromagnetic-field equations," IEEE Trans. Electromagn. Compat., vol. EMC-23, pp. 377-382, Nov. 1981.
[6] Higdon, R. L., "Absorbing Boundary Conditions," J. Computational Phisics, vol. 49, 1986, pp. 437-459.
[7] Betz, V. and R. Mittra, "Comparison and Evaluation of Boundary Conditions for the Absorption of Guided Waves", IEEE Trans. Microwave and Guided Wave Letters, vol. 2, No. 12, 1992, pp. 499-501, Dec. 1992.
[8] Gedney, S. D., "An anisotropic perfectly matched layer absorbing media for the truncation of FDTD lattices," IEEE Trans. Antennas and Propagation, Vol. 44, 1996, pp. 1630-1639.
[9] Sheen, D. M., Ali, S. M., Abouzahra, M. D. e Kong, J. A., "Application of the three-dimensional finite-difference time-domain method to the analysis of planar microstrip circuits," IEEE Trans. On Microwave Theory and Techniques, Vol. 38, N. 7, pp.849-857, Jul. 1990.
[10] Almeida, J. F., Sobrinho, C. L., Santos, R. O. S. "Analysis by FDTD method of a microstrip antenna with PBG considering the substrate thickness variation," Journal of Microwave and Optoeletronics, Vol. 3, N. 3, pp.41-48, Dec. 2003.